Pressure-induced amorphisation and a new high density amorphous metallic phase in matrix-free Ge nanoparticles

N. R. C. Corsini,[†] W. R. Little,[‡] A. Karatutlu,[‡,#] Y. Zhang,[‡] O. Ersoy,[‡] P. D. Haynes,[†] C. Molteni,[¶] N. D. M. Hine,[§,@] I. Hernandez,[‖] J. Gonzalez,[‖] F. Rodriguez,[‖] V. V. Brazhkin,[⊥] and A. Sapelkin[*,‡]

†*Department of Physics, Blackett Laboratory, Imperial College London, Exhibition Road, London, SW7 2AZ, UK*

‡*School of Physics and Astronomy, Queen Mary University Of London, Mile End Road, London, E1 4NS, UK*

¶*Department of Physics, King's College London, Strand, London, WC2R 2LS, UK*

§*TCM Group, Cavendish Laboratory, University of Cambridge, JJ Thomson Avenue, Cambridge, CB3 0HE, UK*

‖*Malta Consolider Team, Departmento CITIMAC, Universidad de Cantabria, Avenida Los Castros s/n, 39005 Santander, Spain*

⊥*High Pressure Physics Institute, RAS, 142190, Troitsk, Moscow Region, Russia*

#*Electrical and Electronics Engineering, Yildirim Campus, Bursa Orhangazi University, 16245, Yildirim, Bursa, Turkey*

@*Department of Physics, University of Warwick, Coventry, CV4 7AL*

E-mail: a.sapelkin@qmul.ac.uk

Abstract

Over the last two decades it has been demonstrated that size effects have significant consequences for the atomic arrangements and phase behaviour of matter under extreme pressure. Furthermore, it has been shown that understanding of how size affects critical pressure-temperature conditions provides vital guidance in the search for materials with novel properties. Here we report on the remarkable behaviour in small (under ~ 5 nm) matrix-free Ge nanoparticles under hydrostatic compression that is drastically different from both larger nanoparticles and bulk Ge. We discover that the application of pressure drives surface-induced amorphisation leading to Ge–Ge bond over-compression and eventually to a polyamorphic semiconductor-to-metal transformation. A combination of spectroscopic techniques together with *ab initio* simulations were employed to reveal the details of the transformation mechanism into a new high density phase—amorphous metallic Ge.

Introduction

It is well known that size effects at the nanoscale can have significant consequences on the mechanical behaviour and structural properties of materials. These effects result in values of phase transition pressures, transformation paths and conditions of stability of phases all being drastically affected.[1] Hence, the subject of behaviour of nanoscale systems under high pressure has been receiving increasing attention since early experiments by Brus[2] and Tolbert *et. al.*[3] Experimental work has in turn stimulated development of theoretical description of the behaviour of nanoscale materials under compression. The importance of surface energy has been emphasised in the early thermodynamic models that have been further developed to account for particle shape,[2,3] surface and interface[4] effects. Crucially, it has been suggested[2] that size effect can be exploited to recover various metastable phases at ambient conditions, giving an access route to novel materials. Furthermore, it has been recently demonstrated that below some critical particle size there may be an increased tendency for pressure-induced amorphisation in nanoparticles.[5–9]

The phenomenon of pressure-induced amorphisation is of interest from the practical as it provides access to structures with novel electronic, optical and mechanical properties. From the fundamental viewpoint, the phenomenon of high pressure amorphisation enables one to explore thermodynamics and kinetics of transformations in metastable systems and has been extensively studied since early work in the 1980s on Si and Ge by Minomura[10] and on ices by Mishima.[11] It has been shown that low temperatures and/or fast decompression rates can be used to access metastable phases and study crystalline-to-amorphous and low density amorphous (LDA) to high density amorphous (HDA) transitions. Pertinent still, the size effect has been successfully exploited by Mishima to suppress crystallisation and to achieve amorphisation of ice through compression of water emulsion.[12]

Despite these advances, observing and studying amorphisation in simple systems such as the technologically important Si and Ge has remained a challenge. In these materials pressure-induced transitions are martensitic-like[13] and kinetically-driven in that local atomic displacements are accompanied by nucleation and growth of the new phase and large (~ 20 %) volume changes. It has thus been a challenge to observe experimentally LDA–HDA transitions in these systems due to the unfavourable transition kinetics that results in amorphous-to-crystalline phase transformations.[10,11,14] In the case of Ge, experimental Raman data collected for bulk a-Ge[7] seem to suggest indirectly a transformation scenario similar to bulk a-Si[6] and porous Si[5] where the metallic HDA phase was assumed to be structurally close to the metallic liquid at the corresponding value of pressure. This is in good agreement with computer simulations for small Si nanocrystals[15–17] and bulk a-Si.[18] However, combined Raman and EXAFS measurements in a-Ge thin films[19] and recent x-ray diffraction experiments with Ge nanoparticles[20] (with sizes between 13 nm and 100 nm) suggest metallisation into an HDA phase that is close or identical to the β-Sn type Ge. This is in line with the computer simulations[21] for bulk a-Ge showing a large volume change ($\sim 19\%$) and a sharp increase in the average interatomic distance. Thus, the subject of amorphisation and the LDA–HDA transition in these systems remains controversial both in bulk samples

and in nanoparticles (see, for example McMillan *et. al.*[5,6] and Garg *et. al.*[22]).

In this work we show that within a certain size regime the size effect can be harnessed to suppress the the diamond-to-β-Sn transformation in small Ge nanoparticles. Thus, for the first time we conclusively study the amorphisation to a metallic HDA and a polyamorphic transformation between LDA and HDA in a simple nanoscale system.

Results and discussion

Experimental measurements were performed on colloidal suspension of Ge nanoparticles with the average diameter of ~ 4 nm (with sizes ranging[23] from 2.3 nm to 5 nm). Optical transmission data as a function of pressure can be seen in Fig. 1a. The data clearly show significant changes in Ge band gap at ambient conditions (translucent orange) as compared to bulk Ge (metallic grey, $E_g = 0.66$ eV, 1900 nm). Furthermore, visual observations show the onset of changes in the translucent phase as it grows increasingly opaque after 14.8 GPa, while in bulk Ge the transition to the metallic β-Sn phase occurs around 10 GPa.[24]

In order to follow structural changes in the semiconducting phase we recorded Raman spectra around the peak corresponding to the zone centre TO-like mode (at around $300\ \mathrm{cm}^{-1}$) in diamond-type Ge (c-Ge) structure as a function of pressure. The evolution of the Raman spectrum of the colloidal sample under pressure is shown in Fig. 1b. The Raman peak at ambient pressure is down-shifted (as compared to bulk c-Ge) and shows an asymmetric shape usually observed in nanostructures. This shift and asymmetry as well as an increased peak width as a function of nanocrystal size are generally understood in terms of phonon confinement effects.[25] Closer analysis reveals that this peak can be seen up to 17.5 GPa, while the semiconductor-to-metal transition in c-Ge at around 10 GPa results in the loss of the Raman signal.[26] Amorphous bulk Ge (a-Ge) can transform at even lower pressures of ~ 6 GPa[14] (although transition has also been observed between 8 GPa[19] and 11 GPa[7]). The Raman signal becomes undetectable above 18 GPa and no new clear signal appears,

4
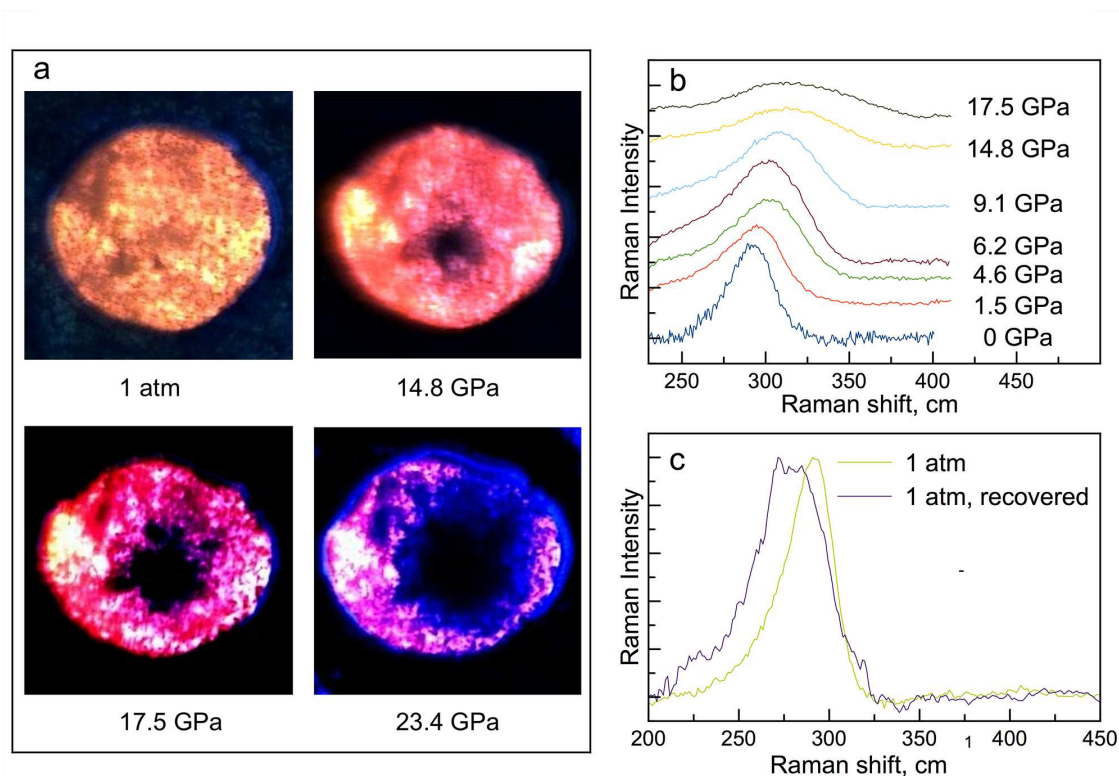
Figure 1: **Light transmission and Raman data. a**, white light transmission through the sample as a function of pressure. **b** evolution of the Raman signal and **c**, comparison of the Raman signal before application of pressure and after pressure release. The Raman signal is lost above 17.5 GPa. The recovered sample shows a broader Raman signal that is also downshifted suggesting an increase in structural disorder.

pointing to transformation into a metallic state. This scenario is also consistent with the optical transmission and PL data, where the PL signal is lost above 17.5 GPa as seen in Fig. 2b, suggesting closure of the band gap. Both the Raman signal and PL as well as the visual appearance of the samples are recovered on pressure release; however, the Raman signal shows a down-shift and an increased broadening for the recovered sample (see Fig. 1c) indicating a higher degree of disorder.

Further analysis of the Raman data shows an unusual feature—a highly non-linear pressure dependence of the peak position as compared to the one observed in the bulk material: see Fig. 2a, where the bulk Ge peak position, extrapolated beyond the diamond-to-β-Sn transition, is also shown. This non-linear behaviour has been reported previously[27] in porous Ge in a similar size regime and was attributed to surface-related reconstruction effects. Here we also examined the Raman peak width and found a clear increase in the full width at half maximum as a function of pressure (inset in Fig. 2a), which suggests an increase in the degree of structural disorder as the pressure is raised. We believe that the observed non-linear behaviour is the combination of two distinct effects: (i) up-shift of the peak under applied pressure due to reduction in Ge–Ge distance and (ii) down-shift due to disorder and increasing contribution from the low wavenumber side of the peak. Thus the peak broadening together with a non-linear pressure dependence point to the gradual amorphisation of the diamond-type structure on pressure increase.

In order to follow the structural evolution of the sample directly to above 18 GPa we extracted information about the short-range order from the extended x-ray absorption fine structure (EXAFS) data. The results of the data analysis are shown in Fig. 3 and compared to previous results for bulk c-Ge[28] and a-Ge.[19] The difference in the behaviour of Ge–Ge distance as compared to the previous reports is drastic. We observe no sharp change in the distance throughout the whole pressure range. Application of pressure eventually results in compression of the bond beyond the stability value for the diamond-type c-Ge structure (see Fig. 3a). This suggests that the proposed metallisation takes place within a local structure

similar to diamond-type Ge and is primarily driven by bond over-compression rather than by structural changes into the octahedral β-Sn arrangement as has been observed in c-Ge and in a-Ge. EXAFS data show that the sample remains disordered up to 24 GPa and that a slight increase in the average coordination number can be observed above 18 GPa (see Fig. 3c). The values of mean squared relative displacements of Ge atoms (see Fig. 3b) show no decrease with applied pressure and thus indicate an increase in disorder, corroborating the gradual amorphisation scenario based on the Raman data.
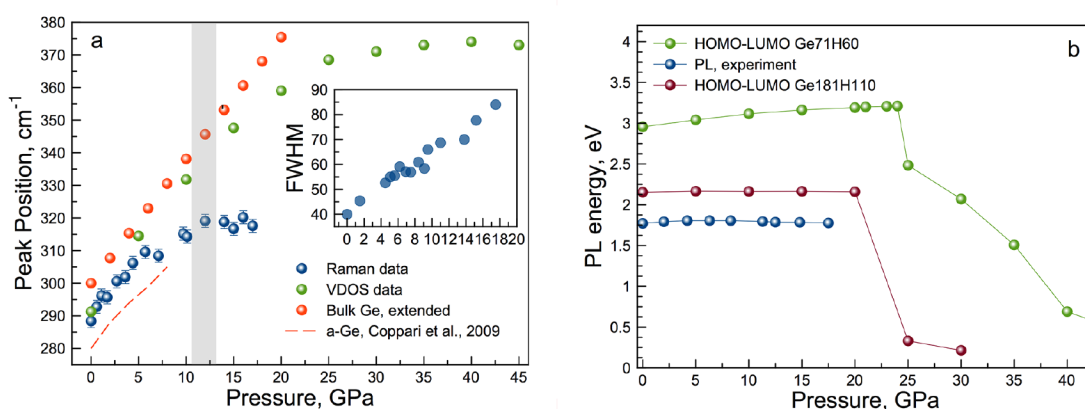

Figure 2: **Analysis of the Raman data together with the photoluminescence data compared with HOMO–LUMO gap. a**, position of the Raman peak extracted from the experimental data (blue circles) together with the maximum of the simulated VDOS (green circles). The data are compared to the Raman peak position for bulk c-Ge (red circles) linearly extrapolated beyond 11 GPa. Inset shows the pressure dependence of the FWHM of the experimental Raman peak. **b**, pressure dependence of the photoluminescence peak position (blue circles) compared to the calculated HOMO–LUMO gaps for $Ge_{71}H_{60}$ (green circles) and $Ge_{181}H_{110}$ (purple circles) hydrogen-terminated clusters.

To gain further understanding of the structural evolution under pressure on the atomic scale, we performed calculations using an implementation of an electronic enthalpy method[29] for simulating finite systems under pressure that we have implemented[17] in ONETEP,[30] a linear-scaling DFT code. As a representative model of a H-terminated Ge nanoparticle we studied the $Ge_{71}H_{60}$ system with the c-Ge structure. The structure of the nanocrystal was initially optimised at 0 GPa and then pressure was applied in steps of 5 GPa or less to find the minimum enthalpy configuration. To make further contact with the experiment,

the HOMO-LUMO gap and the vibrational density of states (VDOS) was calculated on the relaxed structures using density-functional perturbation theory implemented in the plane-wave DFT code CASTEP.[31] Starting from an ordered configuration allows us to better identify signatures of structural disorder in the experimental data.

Simulations clearly show an onset of amorphisation at around 25 GPa (see Fig. 3d). Comparisons of the data obtained from simulations with the experimental results are shown in Figs. 2 and 3. Other than the overestimation of the transformation pressure, which is expected due to the lack of dynamical effects in these simulations and the smaller system size, the observed trends with pressure of the Ge–Ge bond length and coordination numbers and the VDOS peak position (corresponding to optical phonon modes) are all consistent with the experimental data. The same is true for the HOMO–LUMO gap (Fig. 2b). While it is well-known that DFT in the local density approximation employed here underestimates band gaps, this is not immediately apparent for the very small nanocrystals simulated here due to confinement effects. Still, we expect our simulations to give a correct description of relative trends and qualitative behaviour with pressure (see previous work[32] for a comparison of GW and LDA gaps vs volume for Si). Our HOMO–LUMO data exhibit a sharp reduction in the energy value of the gap but we do not observe gap closure (metallisation) above 25 GPa, again most likely due to the pronounced confinement effects for the small system sizes (~ 1.4 nm) studied by our *ab initio* simulations compared to experiments. Indeed, it has been previously demonstrated,[17,33] that particle size can have a significant effect on the value of the gap for Si clusters under the same pressure loading conditions leading to gap closure as the size is changed from ~ 1.3 nm to ~ 2.2 nm. We expect a similar tendency in the H-terminated Ge nanocrystals studied here and indeed simulations of HOMO–LUMO behaviour performed on the larger $Ge_{181}H_{110}$ nanocrystal of ~ 2.3 nm diameter (which overlaps with the smallest experimental sizes[34]) fully confirm this and further support interpretation of the optical transmission and of the photoluminescence data (see Fig. 2b).

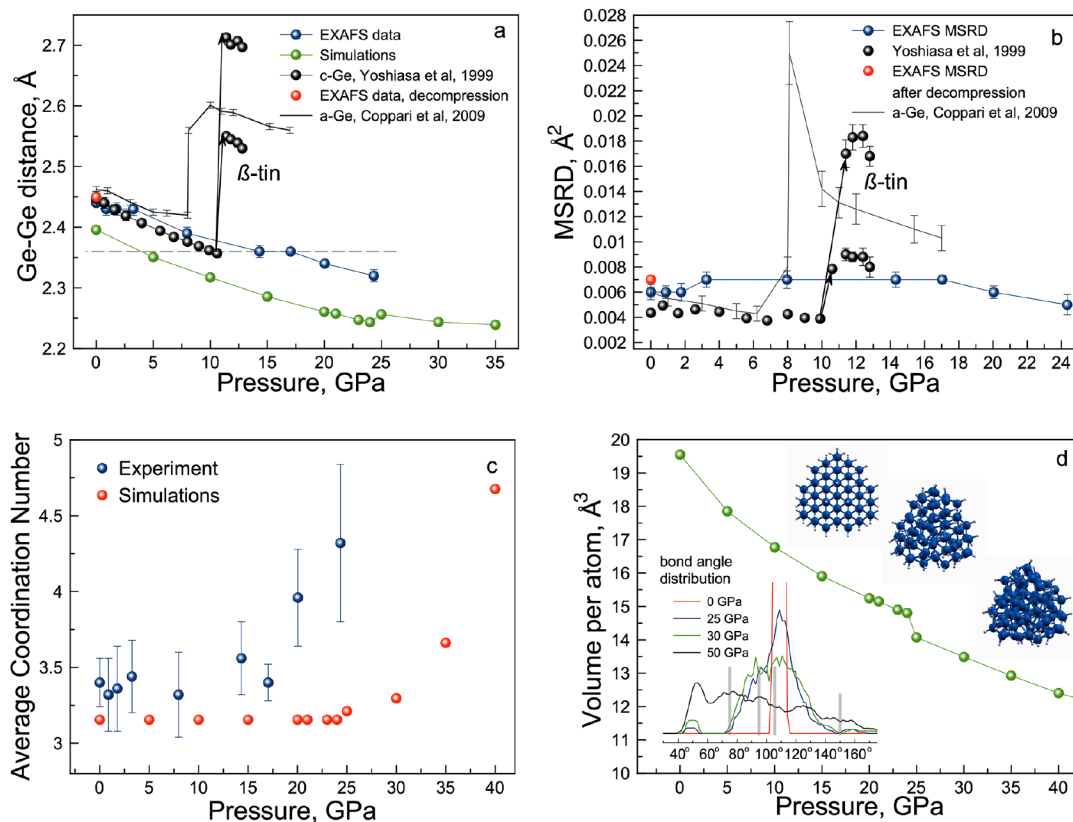Owing to the better level of atomic details of the system evolution that can be obtained

Figure 3: **Structural data obtained from our EXAFS experiments and *ab initio* calculations compared to previously reported data for c-Ge and a-Ge. a**, Ge–Ge average nearest-neighbour distance extracted from EXAFS data in this work (blue circles) and from *ab initio* calculations (green circles). Previously reported data for a-Ge (black line) and c-Ge (black circles) are given for comparison. The horizontal dashed line indicates the value of stability of Ge–Ge distance in c-Ge. **b**, mean squared relative displacements of atoms extracted from EXAFS data in this work (blue circles) compared to the previously reported data. **c**, average coordination numbers extracted from simulations and from EXAFS experiments. **d**, pressure dependence of the calculated volume per atom. Corresponding changes in the structure of $Ge_{71}H_{60}$ cluster and the evolution of the bond angle distribution are also shown (grey bars correspond to the β-Sn structure).

from simulations as compared to experiments, we can see that there is a distinct, if only very small, increase in the the average interatomic distance during transformation to the high density amorphous (HDA) state at 25 GPa. This small discontinuity is consistent with the experimental data at around 15 GPa and is accompanied by a small ($\sim 5\%$) volume decrease at transformation (see Fig. 3d). Thus, both simulations and experimental results show that a transformation into an amorphous phase takes place with relatively small volume jump at transition pressure. In experiment, the transformation follows through LDA–HDA path, while in simulations the path is from c-Ge to HDA.

In bulk Si and Ge systems LDA to HDA transitions are usually interpreted[5,6] by their relationships to the corresponding liquid-liquid LDL–HDL transitions following the approach proposed by Aptekar[35] and the early experimental work by Mishima *et. al.*[11] Ge is one of a number of solids (including ice and Si) that contract on melting and whose melting temperatures fall as pressure rises. This led to the suggestion by Mishima *et. al.*[11] that if such a solid is compressed at a temperature sufficiently low to prevent transformation to another crystalline phase, then for kinetic reasons it may "cold melt" into an amorphous solid on reaching the boundary of absolute instability—a spinodal. The appeal of this thermodynamic approach is in its universality: while equilibrium thermodynamic concepts cannot strictly be applied to bulk amorphous materials and nanoparticles, thermodynamic quantities such as Gibbs free energies can be calculated and guide understanding of transitions in these systems.[5,7,9]

From the thermodynamic point of view the similarity in the high pressure behaviour of amorphous Ge, Ge nanoparticles and liquids is not entirely coincidental. All have higher values of Gibbs free energy than their bulk crystalline counterpart, albeit in the liquid this is due to the high temperatures involved, in an amorphous system - due to structural disorder, while in the nanoparticle it is due to the small systems size and the surface energy contribution. It follows, that this higher value of Gibbs free energy in the size-dependent energy landscape of all possible atomic arrangements (both stable and metastable) may

lead to the new pathways resulting in novel crystalline-to-amorphous and amorphous-to-amorphous transformations.

Despite similarities in the thermodynamic behaviour between LDA–HDA and LDL–HDL transitions, on the atomic level the mechanism of a each pathway is, of course, distinct. This limits the application of essentially macroscopic thermodynamic approaches as differences between various phases are not easily quantifiable and free energies for most part are not known. This led to the adaptation of a percolation-based approach in the framework of Ginzburg-Landau theory to describe process of amorphisation in nanoparticles under compression.[9] This approach successfully explains several key features of high pressure transformations in nanoparticles in terms of defect density and particle size. It also predicts prevalence of pressure induced amorphisation in small nanoparticles and shows that crossover should exist from polymorphic transitions to amorphisation as particle size is reduced. However, while this theory does predict correctly the size dependence of transition pressure in larger particles[20] (up from 10 GPa for bulk to 16.4 GPa for 13 nm particles) and crossover from polymorphic to amorphisation regime observed in our experiments with smaller ($\sim$ 4nm) particles, it also predicts a reduction in amorphisation pressure compared to the polymorphic transition pressure.[9] This is in contrast with our findings. We put the value of the transformation pressure at around 17.5 GPa in experiment and note a tendency for transition pressure to increase further in our calculations as particle size is reduced (see Fig. 2b). We believe that this discrepancy reflects limitations of mean-field type models to adequately describe the behaviour of small systems where bond and surface geometry can play a significant role. While having an advantage of general applicability to both bulk and nanocrystalline systems, this approach does not take into account details of structural evolution on an atomic scale. Such structural evolution will crucially depend on the motion of surface and interior atoms along the transformation path.

We believe that the amorphisation mechanism we observed can be understood if we look into the details of the structural evolution along the diamond to β-Sn transition path (see

Figure 4 a and b) utilising structural models generated in simulations (Figure 4d, e, f). This

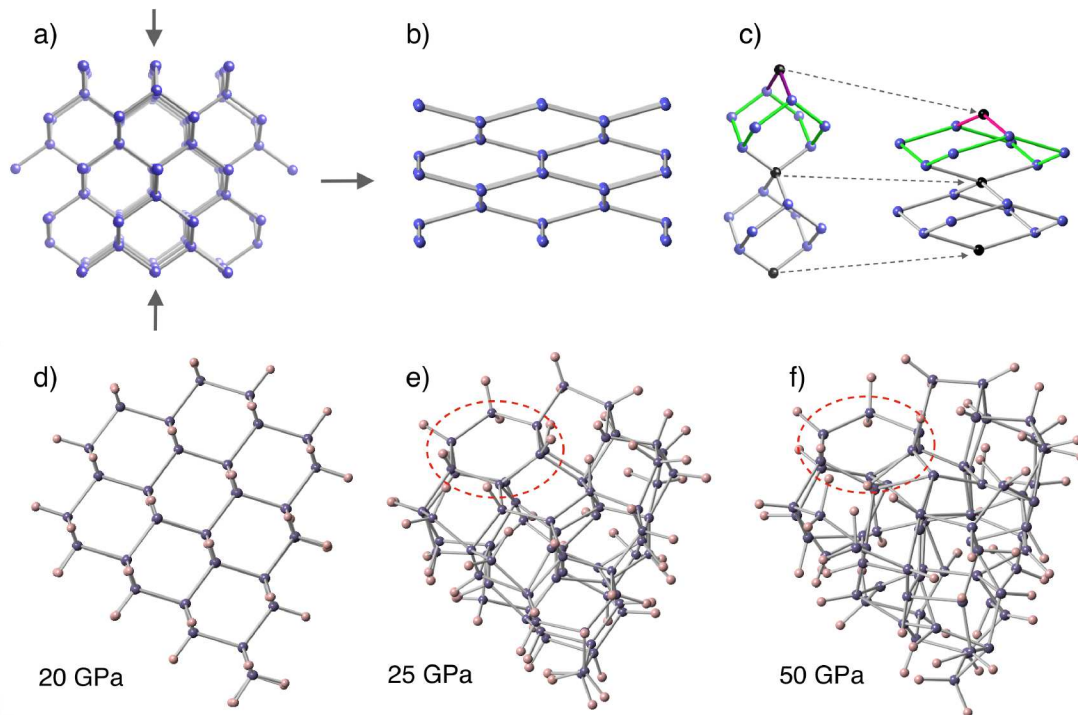Figure 4: **Structural evolution in Ge under high pressure** Diamond-type Ge structure (**a**) transforms to β-Sn structure (**b**) through flattening of the tetrahedral network. The network flattening allows atoms in outer shells (black balls) to be brought closer together (**c**) in the β-Sn structure to accommodate large volume change. This requires opening of the voids through compression and flattening of six-membered rings (green and purple bonds). Structural evolution of the model $Ge_{71}H_{60}$ (**d**) with pressure increase. Evidence of the flattening of the tetrahedral network can be seen (red dashed circle) at 25 GPa (**e**) and at 50 GPa (**f**).

transition in bulk systems proceeds under pressure through flattening of the tetrahedral network by means of an increase in the bond angle from the tetrahedral value ($\sim 109.5°$) to around $150°$ found in the octahedral β-Sn configuration (Durandurdu[36]). This change in the bond angle is required in order to create a sufficiently large void for second nearest neighbours to move in and for the second coordination shell distance to be reduced as a consequence of volume reduction under pressure (Figure 4c). Such rearrangement also results in an increase in the first coordination shell distance after the transition to the β-Sn phase (see Fig. 3a). Creation of such a void and flattening of the tetrahedral network results in a large volume change (~ 19 %) in bulk Ge and in the case of nanoparticles leads to a geometric frustration:

a tendency to increase the surface area while the volume is being reduced. In large Ge particles[20] (13–100 nm) this frustration leads to an increase in the transformation pressure and is eventually resolved through sample fragmentation (most likely initiated at defects and dislocations), surface reconstruction and a change in the crystallite shape following the diamond to β-Sn transition. Such crystallite shape change behaviour has indeed been observed in Si nanoparticles.[3] However, when the particle size is reduced below some critical value, the structural change under hydrostatic compression can only take place through a coherent transformation of the whole of the particle. The result is a compromise: a small volume change (see Fig. 3d) commensurate with the surface reconstruction, all leading to the sample amorphisation. It is at that point that the geometric frustration described above is resolved through transformation into an amorphous metallic phase. Furthermore, analysis of the structural data and of the bond angle distribution in the HDA phase obtained from the simulations (see inset in Fig. 3d) suggest that the structure of this HDA phase has more in common with the corresponding liquid Ge phase[37,38] rather than with β-Sn structure.

Thus, we interpret the experimentally observed pressure-induced transformation reported here as a loss of structural stability and gradual collapse into an amorphous state. In the experiment the onset of amorphisation into the diamond-like LDA phase above 5 GPa is driven by the presence of an amorphous surface layer that acts as a precursor by lowering the energy barrier which otherwise stabilises the c-Ge structure up to 17.5 GPa. This surface-induced amorphisation is followed by a polyamorphic semiconductor-to-metal transformation into a liquid-like HDA phase around 17.5 GPa. This transformation is accompanied by a gradual increase in the coordination number and further decrease in volume. Experimental data and analysis of simulations suggest that the high pressure HDA phase has more in common with liquid Ge rather than with the β-Sn phase. In *ab initio* simulations, where a perfectly ordered H-terminated nanoparticle is selected as a representative system, we observe the diamond-to-HDA transformation.

Conclusions

We clearly show that the size effect can be used successfully to suppress transformation to the β-Sn phase in Ge, to extend the range of stability of the low pressure structure and to effect a transformation to a metallic HDA phase. Furthermore, we demonstrate a very good consistency between *ab initio* simulations and experimental data for Ge. This strongly suggests that similar behaviour should be experimentally observed in small Si nanoparticles under compression as predicted by earlier work[15–17,33] and in other systems and that *ab initio* simulations can help to explore this behaviour for realistic system sizes. Our findings demonstrate that nanoparticle size plays a crucial role in the transformation path and can be used to obtain novel metastable phases under compression. From a wider perspective, this work confirms that the phenomenon of solid state amorphisation may be much more pervasive in small nanoparticles than it is in the bulk, offering new opportunities in production of glassy systems (including metallic ones) and in materials synthesis in general.

Experimental

Hydrogen-terminated matrix-free Ge nanoparticles were prepared by slightly modified[23,34] colloidal route[39] from $GeCl_4$. The samples were translucent orange in appearance and showed a wide photoluminescence peak[23,40] at around 700 nm. The average size of nanoparticles was evaluated by TEM and Raman and was found[23,34] to be 3.9$\pm$0.7 nm. We used a combination of transmission light microscopy, Raman and x-ray absorption spectroscopy (XAS) to follow the structural and electronic changes in Ge nanoparticles under pressure in the diamond anvil cell (DAC). Samples were either loaded into DAC immediately following synthesis or stored in oxygen-free atmosphere to avoid surface oxidation. The usual ruby fluorescence technique was used for pressure measurements. We used methanol-ethanol and silicone oil as a pressure transmitting media to check for possible steric effects. We found no detectable difference between these pressure-transmitting media. X-ray absorption data in a DAC were

collected in fluorescence detection mode to alleviate the problem of diamond reflections tat are particularly severe in this energy range.[41,42] This approach allowed us to collect high quality data out to 12 Å^{-1}. In addition to experiments, we employed *ab initio* simulations using density-functional theory (DFT) as a complementary tool for examining the atomistic details of the evolution of Ge nanocrystals under pressure and the associated changes in their electronic properties.

Ab initio calculations

The structural *ab initio* calculations were conducted with the linear-scaling DFT code ONETEP,[30] using a norm-conserving Ge pseudopotential which retains four valence electrons and a local density approximation for the exchange-correlation functional. ONETEP employs a set of local orbitals, termed non-orthogonal generalised Wannier functions (NG-WFs), which are expanded in a fixed underlying Fourier-Lagrange basis[43] equivalent to a plane-wave basis and independently optimised *in situ*. Nine and one NGWFs are used respectively for each Ge and H atom with a universal NGWF localisation radius $R = 4.23$ Å. The aforementioned pseudopotential, exchange-correlation functional and a plane-wave cutoff of $E_{\text{cut}} = 800$ eV were used for all CASTEP and ONETEP calculations. It has been shown that the two codes give equivalent results under these conditions.[44]

The electronic enthalpy method[29] for simulating finite systems under pressure was used with electronic volume parameters calibrated[17] as $\alpha = 0.0034$ Å^{-3} and $\sigma = 0.00056$ Å^{-3}. The nanocrystals were quasistatically relaxed at different pressures using the quasi-Newton Broyden-Fletcher-Goldfarb-Shanno algorithm for geometry optimisation with tolerances: atomic displacement of 5.3×10^{-3} Å, energy gain per atom of 5.44×10^{-4} eV and maximum force of 5.14×10^{-2} eV/Å.

The coordination numbers were calculated by considering two Ge atoms to be bonded when separated by a distance smaller than the first minimum of the radial distribution function of the bulk: 2.94 Å.

The VDOS calculations were performed with the density-functional perturbation theory module in CASTEP[45] on the relaxed structures at various pressures obtained with ONETEP. The calculations were performed at the Γ-point in a cubic periodic simulation cell of side 20 Å (producing 1 nm vacuum in all directions). Fixed occupancies and the acoustic sum rule correction were applied. For bulk Ge in the equilibrium c-Ge structure, the optical phonon frequency was calculated using a mesh of $8 \times 8 \times 8$ **k**-points to be 295 cm^{-1} (experimental[26] value of 300.6 ± 0.5 cm^{-1} at ambient conditions). The peak corresponding to the TO-like zone center mode of the VDOS, associated with tetrahedral stretching of Ge–Ge bonds, was monitored with pressure and compared to the experimental Raman peak.

Raman and PL measurements

Raman experiments were carried out using a Jobin-Yvon triple monochromator T64000 in subtractive mode, in a configuration including a 1800 grooves/mm grating, a 100 μm slit and a Jobin-Yvon Symphony liquid nitrogen-cooled CCD detector. The total system resolution was < 1 cm^{-1}). An Ar–Kr laser (Coherent Innova) was used at 514.5 and 647.1 nm for Raman, the power was kept low using neutral density filters to avoid heating. The high pressure measurements were performed in a co-focal microscope configuration, with a 20× objective and a membrane driven DAC (culet size 500 μm) employing an Inconel 250 μm thick gasket indented to 75 μm with the hole size 150 μm. The pressure transmitting media were methanol-ethanol mixture or hexane. It was found that the pressure transmitting medium did not affect Raman behaviour. The Raman peak position and peak width were extracted by fitting asymmetric Gaussians to the data. Pressure was determined using the standard ruby fluorescence method. PL experiments were carried out using a Renishaw inVia Raman microscope equipped with 473 nm laser.

X-ray Absorption

High pressure x-ray absorption experiments at the Ge K–edge were carried out at beamline I18 at the Diamond Light Source using a DAC in a set up identical to the one used for Raman data collection. The data were collected in the fluorescence mode to avoid problems with diamond reflections contaminating the x-ray absorption signal. The energy resolution was set to 0.88 eV. Pressure was determined using the standard ruby fluorescence method. Data reduction was carried out using ATHENA[46] package and structural parameters were extracted using the FEFF9[47] code.

Acknowledgement

References

(1) San-Miguel, A. *Chem. Soc. Rev.* **2006**, *35*, 876–889.

(2) Brus, L. E.; Harkless, J. A. W.; Stillinger, F. H. *J. Am. Chem. Soc.* **1996**, *118*, 4834–4838.

(3) Tolbert, S. H.; Herhold, A. B.; Brus, L. E.; Alivisatos, A. P. *Phys. Rev. Lett.* **1996**, *76*, 4384–4387.

(4) Grünwald, M.; Lutker, K.; Alivisatos, A. P.; Rabani, E.; Geissler, P. L. *Nano Letters* **2013**, *13*, 1367–1372.

(5) Deb, S. K.; Wilding, M.; Somayazulu, M.; McMillan, P. F. *Nature* **2001**, *414*, 528–530.

(6) McMillan, P. F.; M. Wilson, D. D.; Machon, D. *Nature Materials* **2005**, *4*, 680–684.

(7) Barkalov, O. I.; Tissen, V. G.; McMillan, P. F.; Wilson, M.; Sella, A.; Nefedova, M. V. *Phys. Rev. B* **2010**, *82*, 020507.

(8) Quan, Z.; Luo, Z.; Wang, Y.; Xu, H.; Wang, C.; Wang, Z.; Fang, J. *Nano Lett.* **2013**, *13*, 3729–3735.

(9) Machon, D.; Mélinon, P. *Phys. Chem. Chem. Phys.* **2015**, *17*, 903–910.

(10) Minomura, S. *J. de Physique* **1981**, *42*, C4–181 – C4–188.

(11) Mishima, O.; Calvert, L. D.; Whalley, E. *Nature* **1984**, *310*, 393–395.

(12) Mishima, O. *Nature* **1996**, *384*, 546–549.

(13) Lyapin, A. G.; Brazhkin, V. V. *Phys. Rev. B.* **1996**, *54*, 12036–12048.

(14) Tanaka, K. *Phys. Rev. B* **1991**, *43*, 4302.

(15) Martoňák, R.; Molteni, C.; Parrinello, M. *Phys. Rev. Lett.* **2000**, *84*, 682–685.

(16) Martoňák, R.; Colombo, L.; Molteni, C.; Parrinello, M. *J. Chem. Phys.* **2002**, *117*, 11329.

(17) Corsini, N. R. C.; Greco, A.; Hine, N. D. M.; Molteni, C.; Haynes, P. D. *J. Chem. Phys.* **2013**, *139*, 084117.
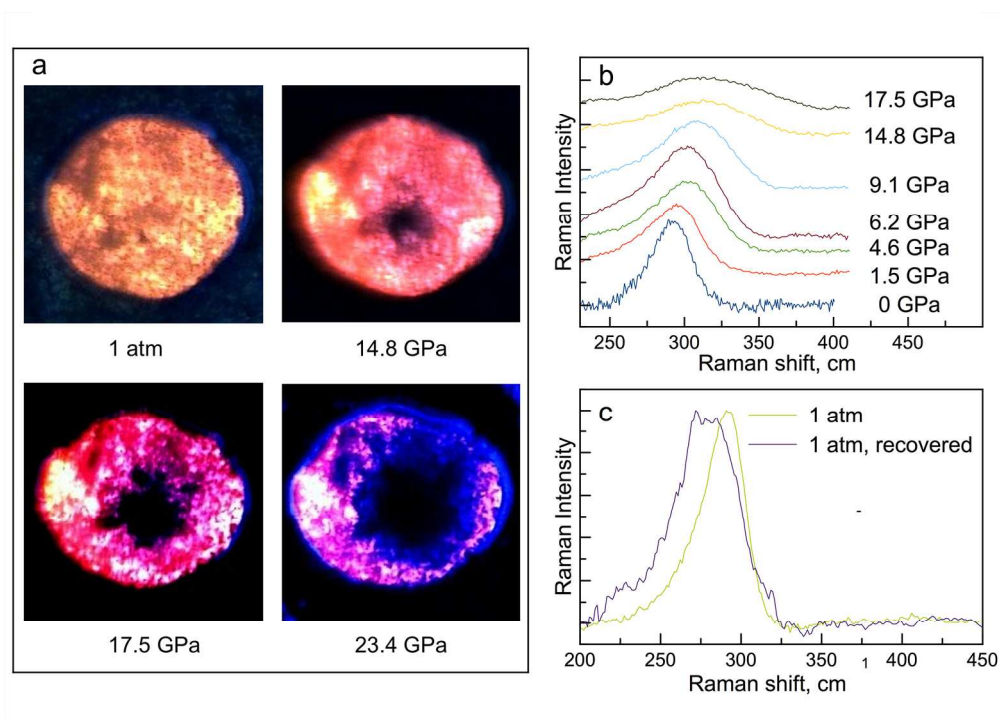
(18) Morishita, T. *Phys. Rev. Lett.* **2004**, *93*, 055503.

(19) Coppari, F.; Chervin, J. C.; Congeduti, A.; Lazzeri, M.; Polian, A.; Principi, E.; Cicco, A. D. *Phys. Rev. B* **2009**, *80*, 115213.

(20) Wang, H.; Liu, J. F.; He, Y.; Wang, Y.; Chen, W.; Jiang, J. Z.; Olsen, J. S.; Gerward, L. *J. Phys. Condens. Matter* **2007**, *19*, 156217.

(21) Durandurdu, M.; Drabold, D. A. *Phys. Rev. B* **2002**, *66*, 041201(R).

(22) Garg, N.; Pandey, K. K.; Shanavas, K. V.; Betty., C. A.; Sharma, S. M. *Phys. Rev. B* **2011**, *83*, 115202.

(23) Karatutlu, A.; Song, M.; Wheeler, A. P.; Ersoy, O.; Little, W. R.; Zhang, Y.; Puech, P.; Boi, F. S.; Luklinska, Z.; Sapelkin, A. V. *RSC Advances* **2015**, *5*, 20566–20573.

(24) Menoni, C. S.; Hu, J. Z.; Spain, I. L. *Phys. Rev. B* **1986**, *34*, 362.

(25) Campbell, I. H.; Fauchet, P. M. *Solid State Commun.* **1986**, *58*, 739–741.

(26) Olego, D.; Cardona, M. *Phys. Rev. B* **1982**, *25*, 1151.

(27) Sapelkin, A. V.; Karavanskii, V. A.; Kartopu, G.; Es-Souni, M.; Luklinska, Z. *Phys. Stat. Solidi (b)* **2007**, *244*, 1376–1380.

(28) Yoshiasa, A.; Nagai, T.; Ohtaka, O.; Kamishima, O.; Shimomura, O. *J. Synchrotron. Rad.* **1999**, *6*, 43–49.

(29) Cococcioni, M.; Mauri, F.; Ceder, G.; Marzari, N. *Phys. Rev. Lett.* **2005**, *94*, 145501.

(30) Skylaris, C.-K.; Haynes, P. D.; Mostofi, A. A.; Payne, M. C. *J. Chem. Phys.* **2005**, *122*, 084119.

(31) Refson, K.; Tulip, P. R.; Clark, S. J. *Phys. Rev. B* **2006**, *73*, 155114.

(32) Godby, R. W.; Needs, R. J. *Phys. Rev. Lett.* **1989**, *62*, 1169.

(33) Molteni, C.; Martoňák, R. *ChemPhysChem* **2005**, *6*, 1765–ÍC1768.

(34) Zhang, Y.; Karatutlu, A.; Ersoy, O.; Little, W.; Cibin, G.; Dent, A.; Sapelkin, A. *J. Sync. Rad.* **2015**, *22*.

(35) Aptekar, L. I. *Sov. Phys. Dokl.* **1979**, *24*, 993–995.

(36) Durandurdu, M. *Phys. Rev. B* **2005**, *71*, 054112.

(37) Kulkarni, R. V.; Aulbur, W. G.; Stroud, D. *Phys. Rev. B* **1997**, *55*, 6896–6903.

(38) Arnold, A.; Mauser, N.; Hafner, J. *J. Phys.: Condens. Matter* **1989**, *1*, 965–980.

(39) Chou, N. H.; Oyler, K. D.; Motl, N. E.; Schaak, R. E. *Chem. Mater.* **2009**, *21*, 4105–4107.

(40) Little, W.; Karatutlu, A.; Bolmatov, D.; Trachenko, K.; Sapelkin, A. V.; Cibin, G.; Taylor, R.; Mosselmans, F.; Dent, A. J.; Mountjoy, G. *Sci. Rep.* **2014**, *4*, 7372.

(41) Sapelkin, A. V.; c. Bayliss, S. *High Pressure Research* **2002**, *21*, 315–329.

(42) Hong, X.; Newville, M.; Prakapenka, V. B.; Rivers, M. L.; Sutton, S. R. *Rev. Sci. Inst.* **2009**, *80*, 073908.

(43) Baye, D.; Heenen, P.-H. *J. Phys. A: Mathematical and General* **1986**, *19*, 2041.

(44) Skylaris, C.-K.; Haynes, P. D. *The Journal of chemical physics* **2007**, *127*, 164712.

(45) Clark, S. J.; Segall, M. D.; Pickard, C. J.; Hasnip, P. J.; Probert, M. I. J.; Refson, K.; Payne, M. C. *Zeitschrift flŹr Kristallographie* **2005**, *220*, 567–570.

(46) Ravel, B.; Newville, M. *J. Sync. Rad.* **2005**, *12*, 537–541.

(47) Rehr, J.; Kas, J.; Vila, F.; Prange, M.; Jorissen, K. *Phys. Chem. Chem. Phys.* **2010**, *12*, 5503–5513.

1
2
3
4
5
6
7
8
9
10
11
12
13
14
15
16
17
18
19
20
21
22
23
24
25
26
27
28
29
30
31
32
33
34
35
36
37
38
39
40
41
42
43
44
45
46
47
48
49
50
51
52
53
54
55
56
57
58
59
60

Graphical TOC Entry

Some journals require a graphical entry for the Table of Contents. This should be laid out "print ready" so that the sizing of the text is correct. Inside the `tocentry` environment, the font used is Helvetica 8 pt, as required by *Journal of the American Chemical Society*.

The surrounding frame is 9 cm by 3.5 cm, which is the maximum permitted for *Journal of the American Chemical Society* graphical table of content entries. The box will not resize if the content is too big: instead it will overflow the edge of the box.

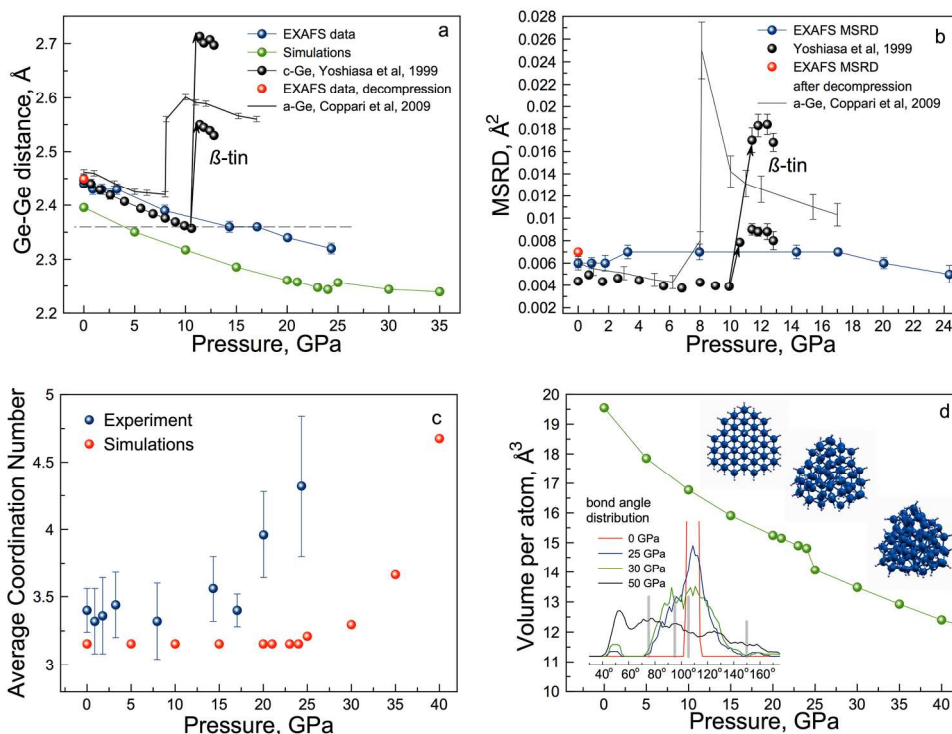This box and the associated title will always be printed on a separate page at the end of the document.

Light transmission and Raman data. a, white light transmission through the sample as a function of pressure. b evolution of the Raman signal and c, comparison of the Raman signal before application of pressure and after pressure release. The Raman signal is lost above 17.5 GPa. The recovered sample shows a broader Raman signal that is also downshifted suggesting an increase in structural disorder.
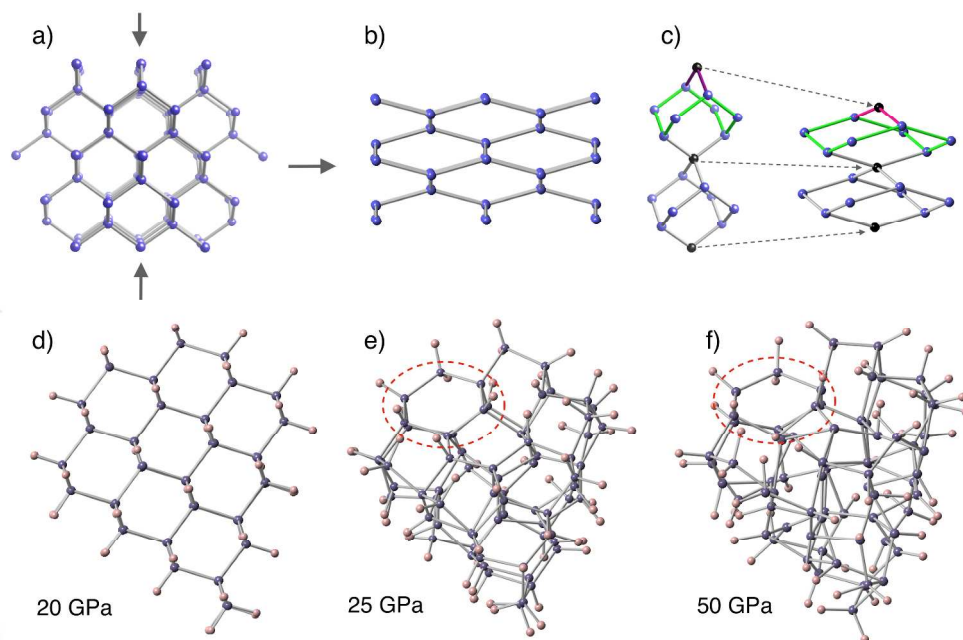705x499mm (72 x 72 DPI)
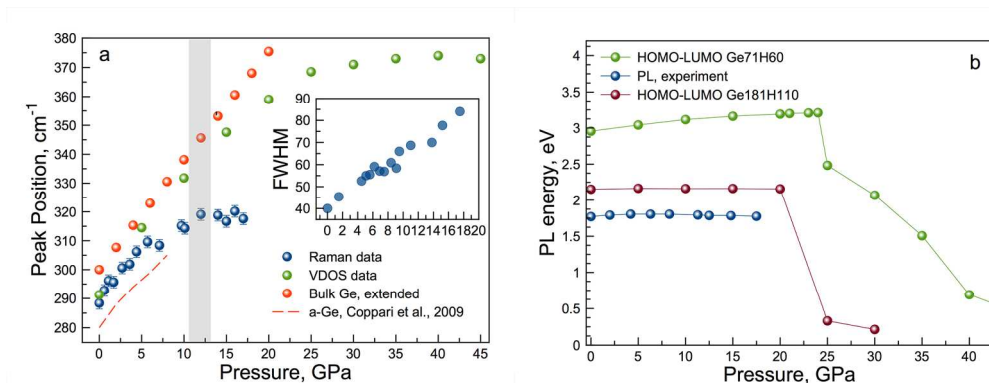
Analysis of the Raman data together with the photoluminescence data compared with HOMO−LUMO gap. a, position of the Raman peak extracted from the experimental data (blue circles) together with the maximum of the simulated VDOS (green circles). The data are compared to the Raman peak position for bulk c-Ge (red circles) linearly extrapolated beyond 11 GPa. Inset shows the pressure dependence of the FWHM of the experimental Raman peak. b, pressure dependence of the photoluminescence peak position (blue circles) compared to the calculated HOMO−LUMO gaps for Ge71H60 (green circles) and Ge181H110 (purple circles) hydrogen-terminated clusters.
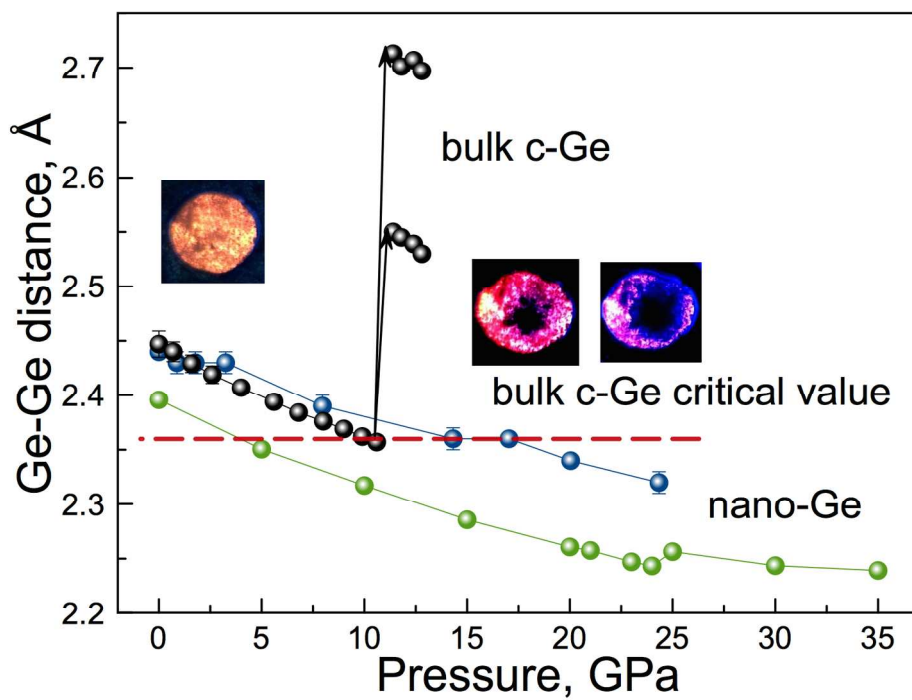740x282mm (72 x 72 DPI)

Structural data obtained from our EXAFS experiments and ab initio calculations compared to previously reported data for c-Ge and a-Ge. a, Ge–Ge average nearest-neighbour distance extracted from EXAFS data in this work (blue circles) and from ab initio calculations (green circles). Previously reported data for a-Ge (black line) and c-Ge (black circles) are given for comparison. The horizontal dashed line indicates the value of stability of Ge–Ge distance in c-Ge. b, mean squared relative displacements of atoms extracted from EXAFS data in this work (blue circles) compared to the previously reported data. c, average coordination numbers extracted from simulations and from EXAFS experiments. d, pressure dependence of the calculated volume per atom. Corresponding changes in the structure of Ge71H60 cluster and the evolution of the bond angle distribution are also shown (grey bars correspond to the β-Sn structure).

740x564mm (72 x 72 DPI)

1
2
3
4
5
6
7
8
9
10
11
12
13
14
15
16
17
18
19
20
21
22
23
24
25
26
27
28
29
30
31
32
33
34
35
36
37
38
39
40
41
42
43
44
45
46
47
48
49
50
51
52
53
54
55
56
57
58
59
60

Structural evolution in Ge under high pressure Diamond-type Ge structure (a) transforms to β-Sn structure (b) through flattening of the tetrahedral network. The network flattening allows atoms in outer shells (black balls) to be brought closer together (c) in the β-Sn structure to accommodate large volume change. This requires opening of the voids through compression and flattening of six-membered rings (green and purple bonds). Structural evolution of the model Ge71H60 (d) with pressure increase. Evidence of the flattening of the tetrahedral network can be seen (red dashed circle) at 25 GPa (e) and at 50 GPa (f).
594x377mm (144 x 144 DPI)

666x499mm (72 x 72 DPI)